



Development and Verification of the Dynamic System Code THERMO-T for Research Reactor Accident Analysis

Marat Margulis & Erez Gilad

To cite this article: Marat Margulis & Erez Gilad (2016) Development and Verification of the Dynamic System Code THERMO-T for Research Reactor Accident Analysis, Nuclear Technology, 196:2, 377-395, DOI: [10.13182/NT16-23](https://doi.org/10.13182/NT16-23)

To link to this article: <https://doi.org/10.13182/NT16-23>



Published online: 10 Aug 2017.



Submit your article to this journal [↗](#)



Article views: 25



CrossMark

View Crossmark data [↗](#)

Development and Verification of the Dynamic System Code THERMO-T for Research Reactor Accident Analysis

Marat Margulis and Erez Gilad*

Ben-Gurion University of the Negev, Unit of Nuclear Engineering, Beer-Sheva 84105, Israel

Received January 31, 2016

Accepted for Publication March 4, 2016

<http://dx.doi.org/10.13182/NT16-23>

Abstract — *The application of best-estimate codes [coupled neutron kinetics (NK)/thermal hydraulics (TH)] for safety analyses of research reactors (RRs) has gained considerable momentum during the past decade. Application of these codes is largely facilitated by the high level of technological maturity and expertise that these codes allow as a safety technology in nuclear power plants, and it is largely driven by International Atomic Energy Agency activities. The present study belongs in this framework and presents the development and application of the coupled NK and TH code THERMO-T to the analysis of protected reactivity insertion accidents and loss-of-flow accidents in a typical RR with standard Materials Testing Reactor plate-type fuel elements. The coupling is realized by considering the neutronic reactivity feedbacks of the fuel and coolant temperatures and a heat generation model for the reactor power. The neutron flux in the reactor core is solved by applying point reactor kinetic equations and employing radial and axial power distributions calculated from a three-dimensional full-core model by the continuous-energy Monte Carlo reactor physics code Serpent. The evolution of temporal and spatial distributions of the fuel, cladding, and coolant temperatures is calculated for all fuel channels by using a finite volume time implicit numerical scheme for solving a three-conservation equation model. In this study, additional features, such as critical heat flux ratio prediction and decay heat model, are implemented for both highly enriched uranium and low-enriched uranium cores, and a comprehensive comparison of THERMO-T results is performed against other codes.*

Keywords — *THERMO-T, research reactor, transient analysis.*

Note — *Some figures may be in color only in the electronic version.*

I. INTRODUCTION

Ever since people began utilizing nuclear energy, there has been a need for facilities that would allow testing of new technologies for increasing the efficiency and safety of existing or planned nuclear reactors. To meet this need, a fleet of research reactors (RRs) has been constructed, and according to the International Atomic Energy Agency (IAEA) RR database,¹ this fleet currently consists of 248 operational RRs worldwide.

Research reactors are developed and built primarily as test facilities and neutron generators for a wide range of

scientific, industrial, and medical purposes. Unlike commercial nuclear power plants (NPPs), RRs are characterized by a small core size, low total thermal power [usually not exceeding 100 MW(thermal)], high power density, low fuel and clad temperatures, and low system pressure. Furthermore, the fuel composition, geometric configuration, and ranges of relevant operational parameters differ between NPPs and RRs and require different neutronic and thermal hydraulics (TH) designs.^{2–5} As a result, RRs must meet different safety requirements and maintain unique safety features to ensure their safe utilization in nominal and off-nominal operation conditions and their safe shutdown in cases of emergencies or accidents. The reactor safety analysis report is frequently updated and

*E-mail: gilade@bgu.ac.il

must include the analysis of a wide variety of safety-related scenarios. Furthermore, unlike in commercial NPPs, the uniqueness of each RR and its experimental systems makes the standardization of design, operation, and licensing almost impractical.^{3,6}

During the past decade, the IAEA and others^{2,6-8} have acknowledged the importance of implementing the well-established and mature NPP safety technology in the safety analysis methodology of RRs and reassessed their safety features.⁵ The safety analysis methodology currently employed for existing NPPs is based on a well-established and very active international community of experts, on well-established and proven methods and computational tools including best-estimate codes and uncertainty analysis, on international standardization, and on an extensive and accessible experimental database.^{2,9}

Despite the large number of operating RRs (with 30 more RRs scheduled to be reopened or constructed in the near future) and a long history of operation of these reactors, standardization is still lacking with respect to their safety analysis,⁷ and there is a need to apply the vast knowledge obtained from code development for safety analysis of commercial NPPs to RRs. Recently, the adequacy of applying NPP computational tools to RRs has been addressed in several studies.^{2,6,8} For example, some studies have evaluated the adequacy of calculating TH transients in RRs by using system codes such as RELAP5 (Refs. 4, 5, and 10 through 19), ATHLET (Ref. 20), PARET (Refs. 12, 17, 21), or RETRAC-PC (Refs. 22 and 23). Others focused on coupled neutron kinetics (NK)/TH calculations by using PARCS/RELAP5 (Ref. 24) and COBRA-EN (Ref. 25), while Monet Carlo neutron transport codes for static and burnup calculation have also been examined.²⁶⁻²⁸ The majority of these studies considered the IAEA safety benchmark for the 10-MW(thermal) Materials Testing Reactor (MTR) light water pool-type reactor,^{29,30} which was specified under the program of RR core conversions from highly enriched uranium (HEU) to low-enriched uranium (LEU) cores. This benchmark consists of detailed steady-state and transient NK and TH calculations for a wide range of accident scenarios.

The computational tools mentioned above and their neutron data libraries are usually access restricted and are not available to all researchers in this field due to commercial or intellectual property considerations, among other reasons. However, a number of open-source neutron codes have recently become available for public use, including the OpenMC Monte Carlo-based code,³¹ the Serpent Monte Carlo-based code,^{32,33} and the DRAGON transport code.³⁴ These codes provide solutions for the steady-state neutron transport equation, while Serpent and DRAGON also provide burnup capabilities. The

capabilities of these codes to calculate basic physical characteristics of RRs was examined in recent years^{27,28,35} by using a steady-state benchmark.²⁹ Although the results showed good agreement to the presented benchmark, none of these codes can perform dynamic calculations of safety aspects of RRs, and they are not fitted with a TH solver that can assess the safety characteristics of the examined reactors.

To bridge this gap and be able to perform dynamic calculations of MTR cores under accident conditions, a system code called THERMO-T is being developed at Ben-Gurion University (BGU) of the Negev, Israel. The THERMO-T system code is a time-dependent version of the THERMO module,^{36,37} which was developed as a multichannel, steady-state, nodal solver for reactor thermal analysis, as part of the BGCore system.^{38,39} BGCore couples MCNP4 as a neutronic solver, a depletion solver SARAF, and a TH solver THERMO. Hence, BGCore is a multiphysics package that can perform coupled neutronic-TH burnup calculation to evaluate nuclear fuel cycles. BGCore was verified against well-established multiphysics codes, such as DYN3D (Ref. 40) and SILWER (Ref. 41). The results of these benchmarks indicated that BGCore can be utilized as a reference tool.

The current version of THERMO-T couples between Serpent, a point kinetics (PK) model, and a time-dependent TH solver. The PK model comprises seven equations for prompt and delayed fission power and six equations for decay heat generation. The TH module solves the three balance (mass, momentum, and energy) equation system by utilizing the Semi Implicit Method for Pressure-Linked Equations (SIMPLE) algorithm.⁴²

The present study considers both HEU and LEU cores of the IAEA 10-MW(thermal) MTR. The three-dimensional neutron flux and power distribution, as well as other kinetic parameters and burnup calculations, are performed using Serpent. A comprehensive set of representative reactivity insertion accident (RIA) and loss-of-flow accident (LOFA) transients is calculated using the coupled NK/TH system code THERMO-T. Several studies have addressed this benchmark over the years^{8,43} and showed good agreement with the results of the benchmark. However, these studies assume a pure cosine shape with specified radial, axial, and engineering power peaking factors for the power distribution in the core. The present study examines this approximation using a calculated axial and radial three-dimensional power distribution, by using the Serpent calculation.^{28,44} This shape is then modified according to the PK model as the calculated transients progress. Furthermore, the correct distributions of the power in the core allowed us to extend the simulation from the traditional

two-channel (average and hot) model to a full-core, one-to-one mapping channel model.

The main goal of this study is to evaluate the TH capabilities of the newly developed code by solving the IAEA 10-MW(thermal) MTR dynamic benchmark³⁰ and to study the adequacy of using the Serpent code to obtain the core neutronic parameters. The coupled calculation scheme and the physical and TH models are validated by comparing the results to the IAEA benchmark report as well as to relevant previous studies.^{8,24,43}

This study is the first stage in the ongoing development of a more advanced transient system code for modeling MTR accidents, into which the DYN3D three-dimensional deterministic neutronic nodal diffusion code^{45,46} is to be integrated and utilized as the core NK simulation tool. This paper is a result summary of this stage in the development of the coupled three-dimensional transient code THERMO-T.

II. COMPUTATIONAL TOOLS AND METHODS

The main objective of the code, which is still under development, is to adequately calculate coupled NK/TH transients, such as RIA, LOFA, partial or full channel blockage, and more, in a standard RR. At this stage of its development, the code utilizes a point reactor model to describe the spatial and temporal dynamics of the neutron flux in the reactor core, using neutronic parameters and flux shape functions calculated by the Serpent code, e.g., full-core three-dimensional radial and axial neutron flux and power distributions. The neutronic model also includes a decay heat model. The TH model of the code comprises a primary coolant loop, which includes the core, the piping, a heat exchanger, and a main circulation pump. The core can be represented by any number of channels by applying any desired mapping scheme between fuel channels and TH channels, using the appropriate radial power distribution. At this stage, the TH code solves one-dimensional single-phase steady-state and transient flows, based on three conservation equations for the mass, momentum, and energy; a heat generation model; and heat transfer equations for the fuel and clad.

II.A. The Neutronic Model

The reactor power is derived by solving the PK equations with one prompt and six delayed groups of neutrons,⁴⁷ where the axial and radial power distributions are calculated using Serpent:

$$\frac{dP_F(t)}{dt} = \frac{\rho(t, T_c, T_f, \rho_c) - \beta_{eff}}{\Lambda} P_F(t) + \sum_{i=1}^6 \lambda_i c_i \quad (1)$$

and

$$\frac{dc_i(t)}{dt} = \frac{\beta_i}{\Lambda} P_F(t) - \lambda_i c_i(t), \quad (2)$$

where

P_F = reactor fission power

β_{eff} = delayed neutron fraction

Λ = prompt neutron generation time

ρ = total reactivity

β_i = relative delayed neutron fraction of group i

c_i = precursor concentration of group i

λ_i = decay constant of precursor group i .

However, the power in the core is not determined solely by fission during the transient. In slow transients, such as the slow LOFA (SLOFA), the decay heat generation of the core is of significance. The decay heat model is implemented according to Ref. 48 in the following form:

$$P_D = \sum_{i=1}^7 \beta_{Di} c_{Di} \quad (3)$$

and

$$\frac{dc_{Di}(t)}{dt} = \beta_{Di} \Lambda (P_F - c_{Di}), \quad (4)$$

where

P_D = normalized decay power

c_{Di} = concentration of decay fission products group i

λ_{Di} = decay constant for decay heat fission products group i

β_{Di} = effective fraction of decay fission products group i .

The coupling of the NK model to the TH conditions in the core is realized through the dependence of the total reactivity on the fuel and coolant temperature, i.e.,

$$\rho(t, T_c, T_f, \rho_c) = \rho_{ext} - \alpha_c \Delta T_c - \alpha_f \Delta T_f - \alpha_{\rho_c} \Delta \rho_c, \quad (5)$$

where

ρ_{ext} = induced external reactivity

$\alpha_c, \alpha_f, \alpha_{\rho_c}$ = reactivity feedback coefficients of the coolant temperature T_c ,

fuel temperature T_f , and coolant density ρ_c , respectively

$\Delta T_c, \Delta T_f, \Delta \rho_c$ = deviation of these parameters from the steady-state conditions (i.e., $\Delta T_c = T_c - T_{c,ss}$, etc.).

II.B. The Serpent Code

Serpent is a continuous-energy Monte Carlo neutron transport code with burnup capabilities, which is developed at the VTT research center in Finland.^{32,33} This code enables modeling complicated three-dimensional geometries and easily defines and obtains parameter distribution, such as flux or reaction rates. Serpent was initially developed as an alternative to deterministic lattice physics codes for generating homogenized multigroup constants for reactor analyses with nodal codes. The current version of Serpent supports neutron data libraries based on the JEFF-2.2, JEFF-3.1.1, ENDF/B-VI.8, and ENDF/B-VII evaluated data files. In the current work, we utilize the ENDF/B-VII libraries.

II.C. The TH Model

To calculate the TH conditions in the core, a TH response code was developed at BGU. This code solves the three conservation equations (mass, momentum, and energy) in time and space and allows dividing the core into any required number of channels, from one lumped TH node up to the number of fuel elements (one-to-one mapping), including the ability to calculate an average channel alongside a hot channel. Each channel is divided into a specified number of axial nodes (in this study, each channel was divided into 60 axial nodes, each 1 cm in height).

II.C.1. The Hydraulic Model

The hydraulic model of THERMO-T enables the prediction of the velocity vector and pressure drop distribution in each channel. Furthermore, the code provides the mass flow rate distribution between the different channels of the core. This is made possible by requiring that the pressure drop between all the channels be the same, which is realized through the solution of the continuity and momentum equations [Eqs. (6) and (7)] on each node along the z -axis:

$$\frac{\partial \rho u}{\partial z} = 0 \tag{6}$$

and

$$\frac{\partial}{\partial z}(\rho u u) = \frac{\partial}{\partial z}\left(\mu \frac{\partial u}{\partial z}\right) + \frac{\partial P}{\partial z} + S_{ext}, \tag{7}$$

where

ρ = coolant density

u = coolant velocity

$\frac{\partial P}{\partial z}$ = pressure gradient along the z -axis

μ = viscosity and is assumed to remain unchanged.

It is also assumed that the coolant is a nonviscous, noncompressible fluid such that the viscosity term in Eq. (7) is neglected. Furthermore, there are no external momentum sources in the problem, so it is also neglected. The reduced equation thus becomes

$$\frac{\partial}{\partial z}(\rho u u) = \frac{\partial P}{\partial z}. \tag{8}$$

The SIMPLE algorithm is used to solve Eqs. (6) and (8), as discussed below.

II.C.2. Heat Transfer Model

The hydraulic model presented in Sec. II.C.1 accounts for two of three conservation equations that are solved in the THERMO-T code. The heat transfer model accounts for the energy balance equation, from which the temperature distributions of both fuel and coolant are derived.

To determine the temperature of the coolant, it is necessary to determine the energy balance inside a single node. A schematic view of a typical coolant node is shown in Fig. 1, wherein u is the coolant velocity, Cp is the coolant heat capacity, ρ is the coolant density, $T_{in/out}$ is the coolant temperature at the boundaries of the node, T_c is the average coolant temperature (bulk), and T_{cl} is the temperature of the wall (clad).

The general terms for heat balance on the node are

$$E_{in} + E_{gen} - E_{out} = E_{st}, \tag{9}$$

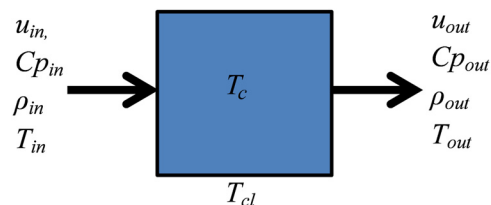


Fig. 1. Schematic representation of a typical coolant node for energy balance.

where

$$\begin{aligned} E_{in} &= \text{energy added to the node} \\ E_{gen} &= \text{energy generated inside the node} \\ E_{out} &= \text{energy removed from the node} \\ E_{st} &= \text{energy stored in the node.} \end{aligned}$$

In our case, there is no generated heat inside the node because all the heat is generated in the inner parts of the fuel. The addition of heat to the node comes from the forced convection mechanism on the fuel surface (clad), whereas the removal of heat from the node is done by the movement of the flow through the node. The final energy balance equation for the coolant node is

$$\begin{aligned} \rho_c C p_c V_c \frac{\partial T_c(z, t)}{\partial t} &= h_{fc} A_f [T_{cl}(z, t) - T_c(z, t)] \\ &\quad - \dot{m} C p_c \frac{\partial T_c(z, t)}{\partial z}, \end{aligned} \quad (10)$$

where

$$\begin{aligned} \rho_c &= \text{coolant density} \\ C p_c &= \text{coolant heat capacity} \\ V &= \text{volume of the node} \\ h_{fc} &= \text{forced convection heat transfer coefficient} \\ A_f &= \text{effective area from which the heat is being removed} \\ \dot{m} &= \text{mass flow rate through the channel.} \end{aligned}$$

The fuel plate consists of fuel meat surrounded by cladding with appropriate dimensions (see Table I), and the coolant channel is defined as the coolant region between two parallel fuel plates. A schematic representation of the fuel and cladding is shown in Fig. 2. Given the dimensions of the fuel plate and the flow conditions, it is reasonable to assume that the heat diffusion rate inside the fuel plate is negligible compared to the time derivative of the fuel enthalpy and the power. Furthermore, in the RIA transient, the convection term on the water side is expected to be much greater than the heat diffusion term in the direction across the fuel plate. This assumption implies a uniform fuel plate temperature in the plane normal to the axial flow direction, leading to vanishing heat conduction terms. The energy balance considerations for the cladding and the fuel are similar, with the addition of a conductive expression in each equation. Therefore, Eq. (9) is still valid for these two regions. It is assumed that the power generated inside the fuel is isotropically distributed, thus facilitating symmetry considerations and the usage of a half-node, as shown in Fig. 2.

It should be noted that THERMO-T has the capability to divide a region into several smaller subregions to obtain a more realistic profile of the temperature distribution. However, the thin cladding and fuel in this benchmark problem make this feature unnecessary. Hence, this model calculates the surface cladding temperature and the average fuel temperature according to

$$\begin{aligned} \rho_{cl} C p_{cl} V_{cl} \frac{\partial T_{cl}(z, t)}{\partial t} &= U A_f [T_f(z, t) - T_{cl}(z, t)] \\ &\quad - h_{fc} A_f [T_{cl}(z, t) - T_c(z, t)] \end{aligned} \quad (11)$$

and

$$\rho_f C p_f V_f \frac{\partial T_f(z, t)}{\partial t} = q(z, t) - U A_f [T_f(z, t) - T_{cl}(z, t)], \quad (12)$$

where

$$\begin{aligned} cl &= \text{cladding} \\ f &= \text{fuel} \\ q(z, t) &= \text{local heat power generated in the fuel through fissions} \\ U &= \text{overall heat transfer coefficient between the fuel and the cladding region, defined according to} \\ U^{-1} &= \frac{d_{cl}}{k_{cl}} + \frac{d_f}{k_f}, \end{aligned} \quad (13)$$

where

$$\begin{aligned} d_{cl}, d_f &= \text{thickness of the cladding and fuel, respectively} \\ k_{cl}, k_f &= \text{heat conduction coefficient of the cladding and fuel, respectively.} \end{aligned}$$

The coupling of the TH model to the NK model is realized through the fission power term $q(z, t)$ appearing in the equation for the fuel temperature.

II.C.3. Critical Heat Flux

The critical heat flux (CHF) is normally the limit of the amount of heat transferred in a nuclear reactor. A mechanical failure of the heated surface might occur once the safety CHF ratio (CHFR) is exceeded. To calculate the CHFR, the 2006 CHF lookup table⁴⁹ is utilized. According to this method, the CHF is obtained from a table in which it is a function of different TH parameters:

TABLE I
Summary of the MTR Core and Fuel Assembly Benchmark Specifications

Benchmark Parameters ²⁹		
Active core height (mm)	600	
Number of axial nodes	61	
Space at the grid plate per fuel element (mm)	77 × 81	
Fuel element (mm)	76 × 80.5 (with support plate) 76 × 80.0 (without support plate)	
Meat dimensions (mm)	63 × 0.51 × 600	
Fuel plate:		
Number per fuel element	23	
Number per control element	17	
Fuel meat thickness (mm)	0.51	
Clad thickness (mm)	0.38	
Fuel active width (cm)	6.30	
Fuel with clad width (cm)	6.65	
Distance between fuel plates (mm)	2.23	
Remaining plate positions of the control element: Four aluminum plates ($\rho_{Al} = 2.7 \text{ g/cm}^3$), each 1.27 mm thick in the position of the 1st, 3rd, 21st, and 23rd standard plate positions; water gaps between the two sets of aluminum plates		
Cladding properties:		
Thermal conductivity (W/mK)	180	
Volumetric heat capacity ($\text{J/cm}^3 \cdot \text{K}$)	$2.0069 + 0.0012T^a$	
Fuel thermal properties:		
Thermal conductivity (W/mK)	HEU	LEU
Volumetric heat capacity ($\text{J/cm}^3 \cdot \text{K}$)	158	50
	$2.0072 + 0.0011T^a$	$1.929 + 0.0007T^a$
Thermal hydraulics conditions:		
Coolant inlet temperature ($^{\circ}\text{C}$)	38	
Coolant mass flow rate (m^3/h)	1000	
Pressure at core height (bars)	1.7	
Neutronic core parameters:		
Delayed neutron fraction	HEU Core	LEU Core
Neutron generation time (s)	7.6071×10^{-3}	7.275×10^{-3}
Doppler feedback coefficient ($\$/^{\circ}\text{C}$)	55.96×10^{-6}	43.74×10^{-6}
Coolant feedback coefficient ($\$/^{\circ}\text{C}$)	3.6×10^{-5}	3.31×10^{-3}
Density feedback coefficient ($\$/\text{g} \cdot \text{cm}^{-3}$)	1.537×10^{-2}	1.082×10^{-2}
	32.57	40.7

^aTemperature in kelvins.

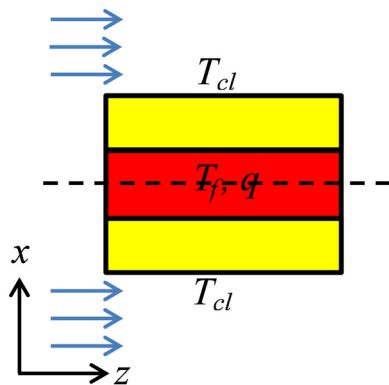


Fig. 2. Schematic representation of a typical fuel and cladding node for energy balance.

$$q''_{CHF} = q''_{CHF}(p, G, X_{eq}, D_{hyd}), \tag{14}$$

where

- p = local pressure
- G = mass flux ($\text{kg/s} \cdot \text{m}^2$)
- X_{eq} = local vapor quality
- D_{hyd} = hydraulic diameter.

The 2006 CHF lookup tables are based on experimental data obtained from a tube with a vertical upward flow of a mixture of steam and water. The range of the data

covered by the lookup tables is wide. The experiments were performed on 8-mm tubes, in a pressure range of 0.1 to 20 MPa, mass flux of 0.0 to 8000 kg/s · m², and vapor quality ranges between -0.5 and 1.0. A linear interpolation is assumed between all the points in the table, and a correction for pipe diameter is applied according to

$$q''_{\text{CHF}} = q''_{\text{CHF}_{8\text{mm}}} \left(\frac{1000D_{\text{hyd}}}{8} \right)^{-0.5} . \quad (15)$$

The 2006 CHF lookup tables were verified against experimental data available for nuclear reactors in several studies.^{50,51}

II.D. Numerical Scheme

II.D.1. Point Kinetics Model

The PK model [Eqs. (1) and (2)] is solved by using the semi-implicit scheme of the form

$$\frac{P_F^{n+1} - P_F^n}{\Delta t} = \frac{\rho^n - \beta_{\text{eff}}}{\Lambda} P_F^n + \sum_{j=1}^6 \lambda_j c_j^{n+1} \quad (16)$$

and

$$\frac{c_j^{n+1} - c_j^n}{\Delta t} = \frac{\beta_j}{\Lambda} P_F^n - \lambda_j c_j^{n+1} , \quad (17)$$

where n denotes the value of the variable at time $t_n = n\Delta t$. The discretization of the PK equations leads to the following iterative procedure at each time step (excluding relaxation factors for clarity):

$$P_F^{k+1} = P_F^k + \Delta t \left(\frac{\rho^n - \beta_{\text{eff}}}{\Lambda} P_F^k + \sum_{j=1}^6 \lambda_j c_j^{k+1} \right) \quad (18)$$

and

$$c_j^{k+1} = \left(c_j^k + \Delta t \frac{\beta_j}{\Lambda} P_F^k \right) \times (1 + \Delta t \lambda_j)^{-1} , \quad (19)$$

where k denotes the iteration index. The iterative process is terminated once the convergence criterion $|x^{k+1} - x^k|/x^k \leq \varepsilon$ is satisfied for a predetermined convergence threshold ε , where x is a vector of variables. The decay heat model [Eqs. (3) and (4)] is solved similarly, according to

$$P_D^{k+1} = \sum_{i=1}^7 \beta_{Di} c_{Di}^{k+1} \quad (20)$$

and

$$c_{Di}^{k+1} = c_{Di} + \Delta t \frac{\beta_{Di}}{\Lambda} (P_F^{k+1} - c_{Di}^k) . \quad (21)$$

Finally, the reactor power is a combination of both fission and decay heat power, with the fraction of the total power contributed by the decay heat assumed to be 6.1% (f_D),

$$P_{\text{tot}} = P_F(1 - f_D) + P_D f_D . \quad (22)$$

However, the presented decay heat model [Eqs. (20) and (21)] is valid mainly for short periods after reactor shutdown. For longer periods, it is suggested to utilize an empirical relation for decay heat⁵²:

$$P_D = 0.1P_0 [(\tau - \tau_s + 10)^{-0.2} - (\tau + 10)^{-0.2} + 0.87 \times (\tau + 2 \times 10^7)^{-0.2} - 0.87(\tau - \tau_s + 2 \times 10^7)^{-0.2}] , \quad (23)$$

where

- P_0 = total power prior to scram
- τ = time elapsed since reactor startup (s)
- τ_s = time elapsed since scram insertion (s).

II.D.2. Heat Transfer Model

The three energy conservation equations [Eqs. (10), (11), and (12)] for the coolant, clad, and fuel are solved in time and space by utilizing explicit temporal and spatial discretization, taking into account changes in different material properties due to temperature and pressure:

$$\rho_f V_f C p_f \frac{T_f^{n+1} - T_f^n}{\Delta t} = q^n - UA_f(T_f^n - T_{cl}^n) , \quad (24)$$

$$\rho_{cl} V_{cl} C p_{cl} \frac{T_{cl}^{n+1} - T_{cl}^n}{\Delta t} = UA_f(T_f^n - T_{cl}^n) - hA_f(T_{cl}^n - T_c^n) , \quad (25)$$

and

$$\rho_c V_c C p_c \frac{T_c^{n+1} - T_c^n}{\Delta t} = hA_f(T_{cl}^n - T_c^n) - \dot{m}Cp_c \times \left(\frac{T_{c,\text{out}}^n - T_{c,\text{in}}^n}{\Delta z} \right) . \quad (26)$$

Equations (24), (25), and (26) are iteratively solved coupled to the mass and momentum equations. The coupling scheme is discussed later in this section. As mentioned above, the solution of the three-equation model

provides a good estimation of the temperature distribution inside the channel.

II.D.3. SIMPLE Algorithm

The SIMPLE algorithm⁵² is an iterative solution of the momentum equation [Eq. (7)] and the continuity equation [Eq. (6)]. The field is divided into two separate fields: velocity and pressure. A typical node grid for the SIMPLE algorithm is shown in Fig. 3, wherein *W*, *E*, and *P* correspond to the points where the pressure field is being solved while *A_w* and *A_e* correspond to the points where the velocity vector is being obtained. The discrete momentum equation is given by

$$a_i u_i^* = \sum_{nb} a_{nb} u_{nb}^* + (P_W^* - P_E^*) A_i + b_i, \quad (27)$$

where

nb = neighboring nodes

a_i, *a_{nb}* = multiplication coefficients of the velocity from the momentum equation [Eq. (7)]

u_i^{*}, *u_{nb}*^{*} = velocities at node *i* and its neighboring nodes

P = pressure at neighboring pressure nodes

A_i = flow area of the node

b_i = free parameter.

A full scheme of the solution of the steady-state problem is shown in Fig. 4, and the time loop is shown in Fig. 5.

The pressure correction equation is susceptible to divergence unless some underrelaxation is used during the iterative process, and a new, improved, pressure *P_{new}* is obtained with

$$P_{new} = P^* + \alpha_p P', \quad (28)$$

where α_p is the relaxation factor of the guessed pressure field *P*^{*}. If the relaxation factor is chosen to be closer to 1, the guessed pressure field is corrected by the correction pressure field *P*'. This process could result in a convergence error if

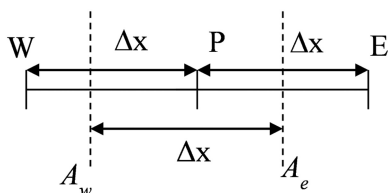


Fig. 3. The grid formation for the SIMPLE algorithm.

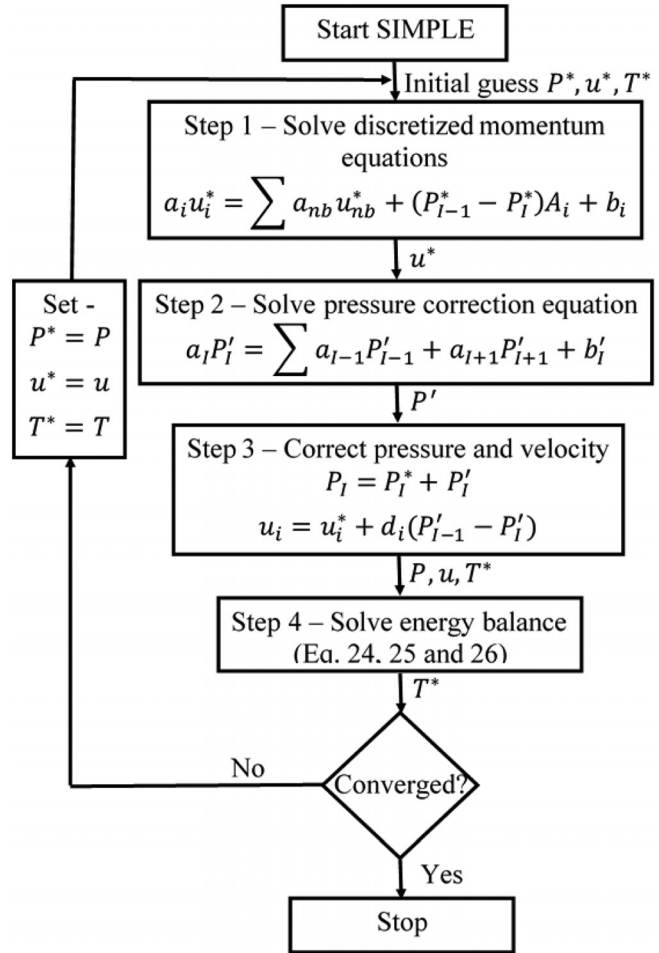


Fig. 4. Flowchart of the steady-state SIMPLE algorithm.

the initial guess of the pressure field significantly differs from the actual result. On the other hand, selecting the relaxation factor to be closer to 0 would result in no correction at all of the initial guess. Therefore, the selection of the relaxation factor should be between 0 and 1, and it should be sufficiently larger than 0 to ensure the correct progression of the solution. The same applies to the velocity, which is also underrelaxed according to

$$u_{new} = \alpha_u u^k + (1 - \alpha_u) u^{k-1}, \quad (29)$$

where

α_u = velocity underrelaxation factor

u^{k-1}, *u^k* = calculated velocities at the previous and current iterations, respectively.

II.E. Coupling Scheme

As stated above, the THERMO-T package couples three tools (Serpent, NK module, and TH module). The

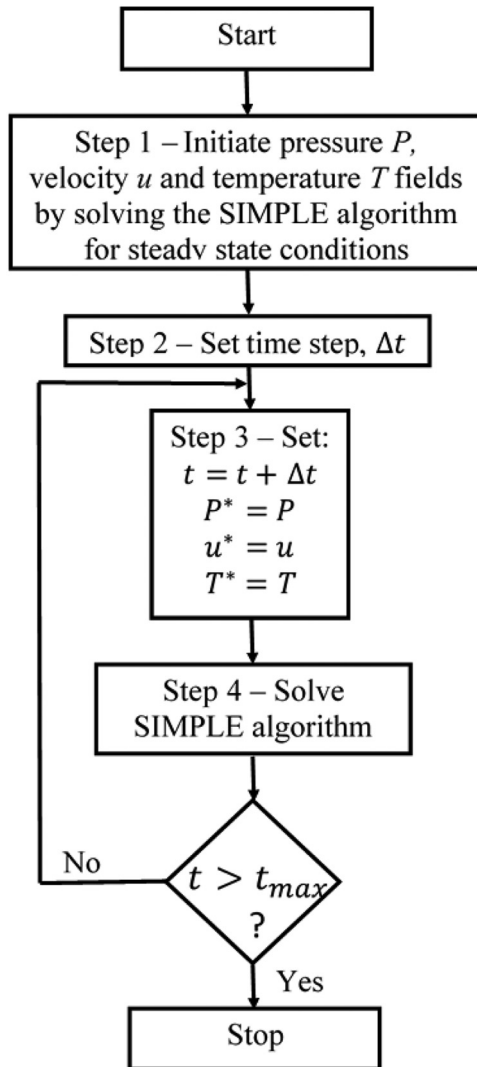


Fig. 5. Flowchart of the time-dependent loop for the SIMPLE algorithm.

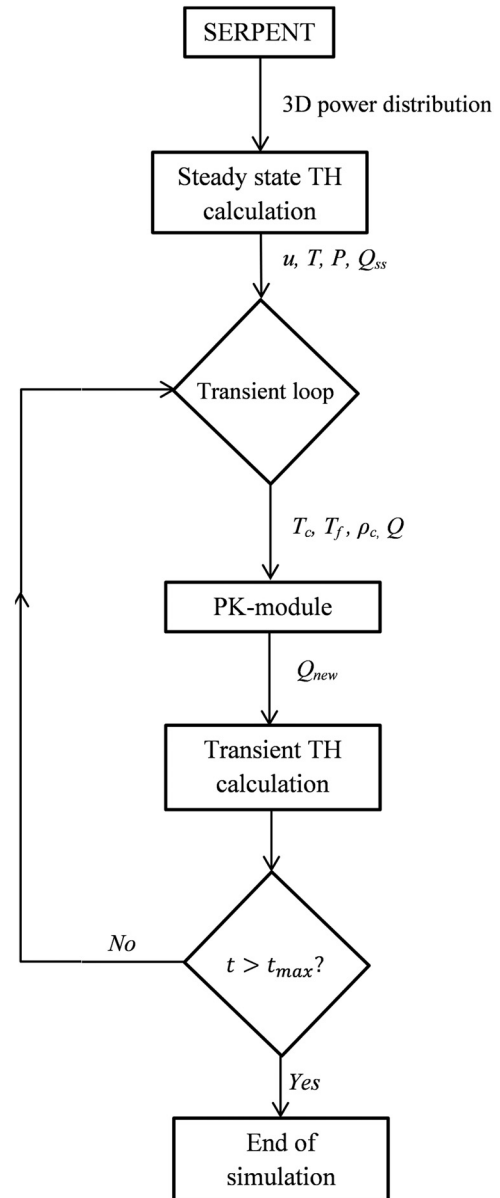


Fig. 6. THERMO-T working coupling scheme.

Serpent code provides an initial distribution of the power inside the core at nominal operation conditions. The three-dimensional power distribution is then fed into THERMO-T, which solves the initial steady-state TH conditions of the core by using the given three-dimensional power distribution and a channel model, e.g., a one-to-one mapping of TH channels to fuel elements, a two-channel model, or lumped-core model. Then, calculation of the next time step begins by solving the new amplitude for the three-dimensional flux shape according to the reactivity changes in the core. This calculation is performed by the NK module, which accounts for reactivity changes via changes in the fuel and coolant temperature, coolant density, and external sources of reactivity. The new power distribution is then transferred to the TH module, which calculates the new distribution of the TH parameters in the

core. The flowchart of the THERMO-T module is shown in Fig. 6.

At each time step, the updated temperatures and local pressure values allow the code to update the coolant properties, which is accomplished using the XSteam module,⁵³ and the clad and fuel properties according to the equations of state provided in the benchmark.³⁰ The XSteam module is a set of steam and water properties' tables, based on IAPWS-IF97 (Ref. 54). It provides properties for steam and water in ranges from 0 to 1000 bars and 0°C to 2000°C. The tables provide a wide range of parameters, e.g., enthalpy, density, and viscosity, for both steam and liquid in all thermodynamic states (subcooled liquid, saturated liquid/vapor, superheated vapor).

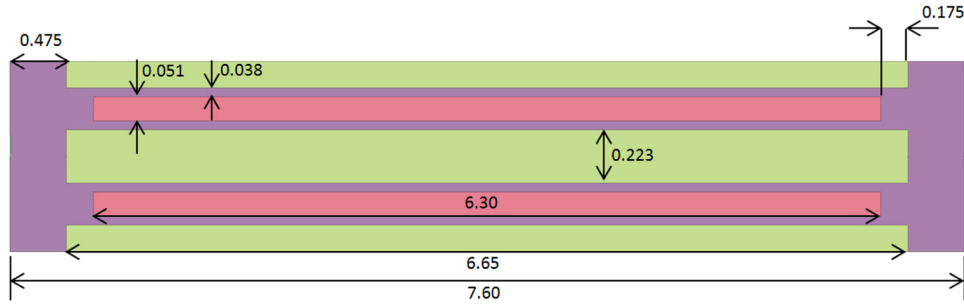


Fig. 7. Geometry and dimensions of a standard fuel element unit cell (in units of centimeters).

The conductivity values of the fuel and cladding are assumed to be constant. However, the volumetric heat capacity ($C_v = \rho_x C_{p_x}$) is temperature dependent. The value of the volumetric heat capacity of the aluminum cladding is calculated according to Eq. (30), whereas for HEU and LEU fuels, the volumetric heat capacity is calculated according to Eqs. (31) and (32), respectively:

$$C_v = 2.069 + 0.0012T_{cl} \quad (30)$$

$$C_v = 2.072 + 0.0011T_f \quad (31)$$

and

$$C_v = 1.929 + 0.0007T_f \quad (32)$$

where

T_x = average temperature of the cladding and the fuel (K)

C_v = volumetric heat capacity ($J/cm^3 \cdot K$).

Finally, the values of the numerical parameters, e.g., time-step size, number of axial nodes, and iterative relaxation parameters, were optimized after careful considerations and repeated trials until the desired accuracy and stability were achieved.

III. BENCHMARK DESCRIPTION

In the current study, both HEU and LEU cores were modeled. The core grid is a 6×5 grid and contains 21 fuel elements and 4 control elements. The geometry and dimensions of a standard fuel element unit cell are shown in Fig. 7. Each standard fuel element comprises 23 fuel plates, whereas the control fuel elements comprise 17 fuel plates, as shown in Fig. 8. The core configuration for both beginning of life (BOL) and end of life (EOL), as a function of depletion, is shown in Fig. 9. The core is reflected on both sides with graphite reflectors, and it is surrounded by water. The active core height of 60 cm is followed, on both sides, by 15 cm of axial Al-H₂O

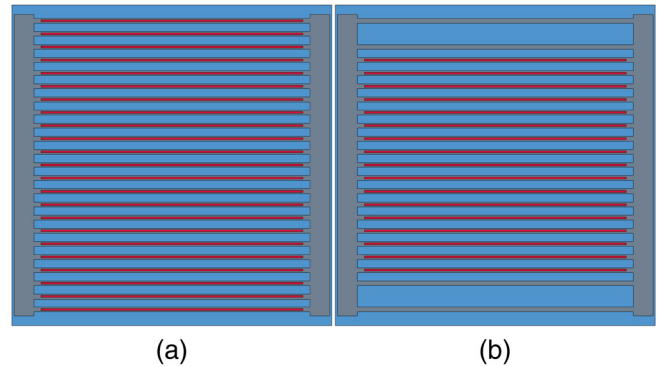


Fig. 8. A midplane XY cross section of (a) standard and (b) control fuel elements, as modeled in Serpent.

Water	Water	Fuel BOL 5% EOL 10%	Fuel BOL 25% EOL 30%	Fuel BOL 5% EOL 10%	Water	Water
Graphite	Fuel BOL 5% EOL 10%	Control BOL 25% EOL 30%	Fuel BOL 45% EOL 50%	Control BOL 25% EOL 30%	Fuel BOL 5% EOL 10%	Graphite
Graphite	Fuel BOL 25% EOL 30%	Fuel BOL 45% EOL 50%	Fuel BOL 45% EOL 50%	Fuel BOL 45% EOL 50%	Fuel BOL 25% EOL 30%	Graphite
Graphite	Fuel BOL 25% EOL 30%	Fuel BOL 45% EOL 50%	Water	Fuel BOL 45% EOL 50%	Fuel BOL 25% EOL 30%	Graphite
Graphite	Fuel BOL 5% EOL 10%	Control BOL 25% EOL 30%	Fuel BOL 45% EOL 50%	Control BOL 25% EOL 30%	Fuel BOL 5% EOL 10%	Graphite
Water	Water	Fuel BOL 5% EOL 10%	Fuel BOL 25% EOL 30%	Fuel BOL 5% EOL 10%	Water	Water

Fig. 9. MTR core configuration for both BOL and EOL as a function of ²³⁵U depletion.

reflectors containing volume fractions of 20% Al and 80% water. A summary of the benchmark parameters is given in Table I.

III.A. Examined Transients

The benchmark problem presented in Ref. 30 consists of two different types of accidents: RIA and LOFA. Both scenarios are examined in fast and slow responses. The transient specifications are detailed in Table II. The RIA

TABLE II
Main Transient Characteristics for the IAEA MTR Benchmark for HEU and LEU Cores

Main Transient Parameters	RIA	LOFA
Initial power	1.0 W	12.0 MW
Steady-state duration time before transient	50 s	50 s
Rate of external reactivity insertion	1.5 $\$/0.5$ s (FRIA) 1.35 $\$/0.5$ s (LEU only) 0.10 $\$/1$ s (HEU only) 0.09 $\$/1$ s (LEU only)	
Loss-of-flow decay period	— —	1.0 s (FLOFA) 25.0 s (SLOFA)
Scram point	12 MW (120% of nominal power)	85% of nominal core coolant flow rate
Delayed period before scram	0.025 s	0.2 s
Shutdown reactivity insertion	-10.0 $\$/0.5$ s	-10.0 $\$/0.5$ s

transient is classified as an overpower transient. This RIA transient is characterized by a prompt power excursion followed by strong reactivity feedback effects related to fuel temperature, coolant temperature, and coolant density changes. Several RIA scenarios are examined in this study, as described in Table II. The LOFA transient is classified as core heatup due to the malfunction of the primary cooling system, while the reactor operates around the nominal power. In this case, the flow decay is modeled as an exponential decrease, $\exp(-t/T)$, with a period T , which equals 1 and 25 s for the fast LOFA (FLOFA) and SLOFA cases, respectively.

IV. RESULTS AND DISCUSSION

IV.A. RIA Results

The results of the fast reactivity insertion of 1.5 $\$/0.5$ s for HEU and LEU cores, and 1.35 $\$/0.5$ s for the LEU core, are shown in Figs. 10 and 11, respectively. The results show that the power peak is reached faster in the LEU core than in the HEU core, due to a shorter neutron generation time in the LEU core, as expected in this case. In fast transients, the strong Doppler feedback in the LEU core leads to a faster decrease in power. Further examination of the minimal CHF (MCHFR) shows that it remains above the minimal value of unity for all cases of RIAs, as shown in Fig. 12.

The slow RIA (SRIA) is shown in Fig. 13. The self-limiting power behavior is observed more vividly in the LEU case, in which the power rise becomes smoother due to the delayed feedback effect of coolant and fuel temperature increase. Furthermore, the MCHFR for the SRIA transients is substantially >1 , as shown in Fig. 14, and no boiling is observed.

A summary of the protected fast RIA (FRIA) and SRIA transients is given in Tables III and IV, respectively. In Tables III and IV, THERMO-T is compared with calculations that were carried out by PARET [Argonne National Laboratory (ANL)], RETRAC-PC [Laboratoire d'Analyse de Sûreté (LAS) (Algeria)], COSTAX-BOIL [Junta de Energia Nuclear (JEN) (Spain)], EUREKA-PT [Japan Atomic Energy Research Institute (JAERI) (Japan)], and COBRA III-C (Interatom) (Germany)], which are presented in the IAEA benchmark.³⁰ Comparisons to benchmark calculations, which were

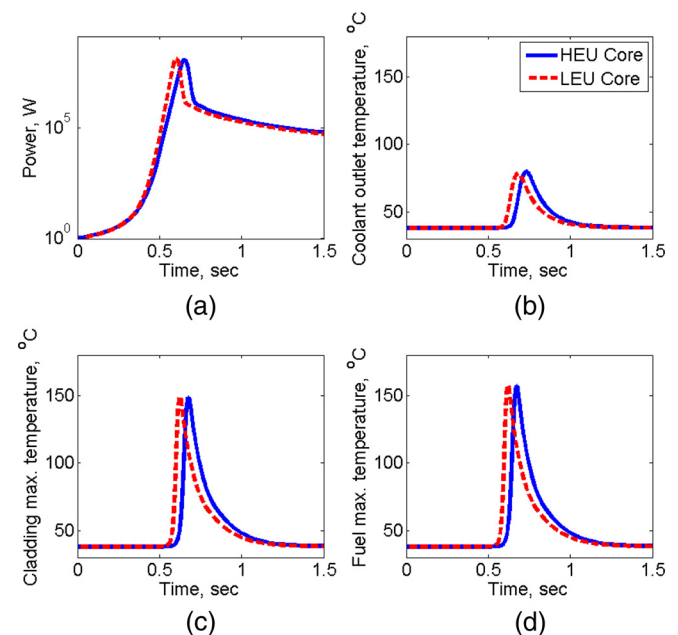


Fig. 10. Transient responses of HEU and LEU benchmark cores to reactivity insertion of 1.5 $\$/0.5$ s: (a) power, (b) coolant outlet temperature, (c) cladding maximum temperature, and (d) fuel maximum temperature.

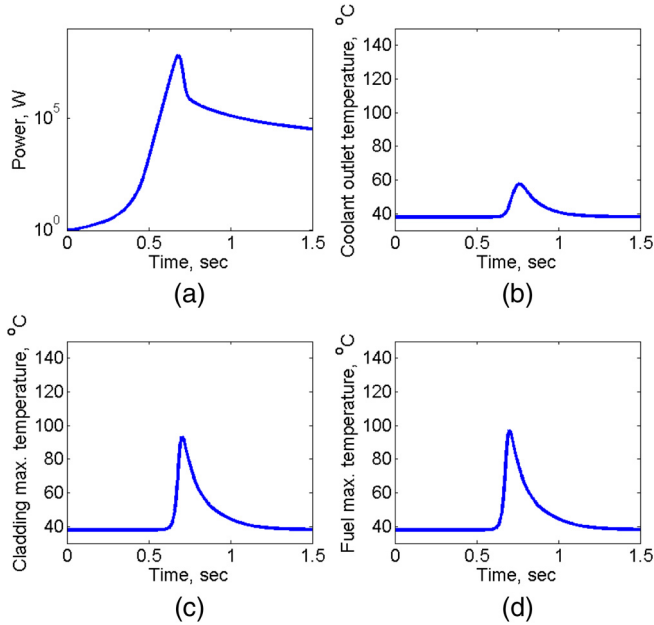


Fig. 11. Transient response of LEU benchmark core to reactivity insertion of 1.35 \$/0.5 s: (a) power, (b) coolant outlet temperature, (c) cladding maximum temperature, and (d) fuel maximum temperature.

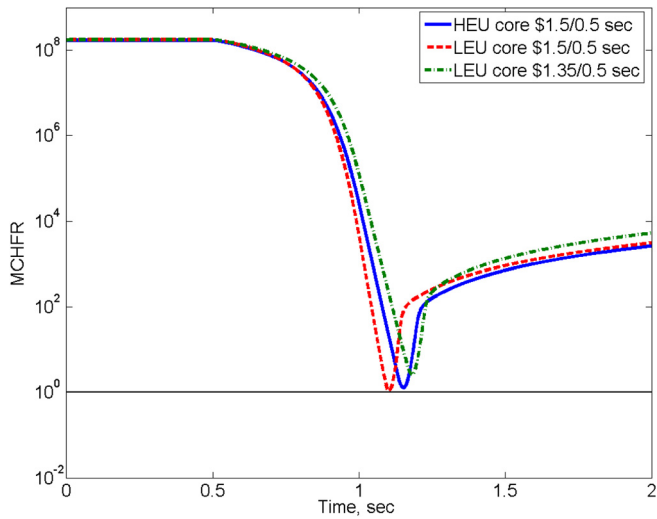


Fig. 12. MCHFR for FRIA transients.

performed with RELAP5/MOD3.2 [University of Pisa (UPISA)] (Ref. 8), are also shown in the summary.

The comparisons in Tables III and IV show that the results obtained by THERMO-T for these transients are in good agreement with the results obtained by various other codes. However, in many cases, the temperatures of the clad surface calculated by THERMO-T seem to be lower than those calculated by other codes. This result can be explained by different peaking factors that are used in THERMO-T. The benchmark-specified values for the radial and axial peaking factors are 1.4 and 1.5, respectively.

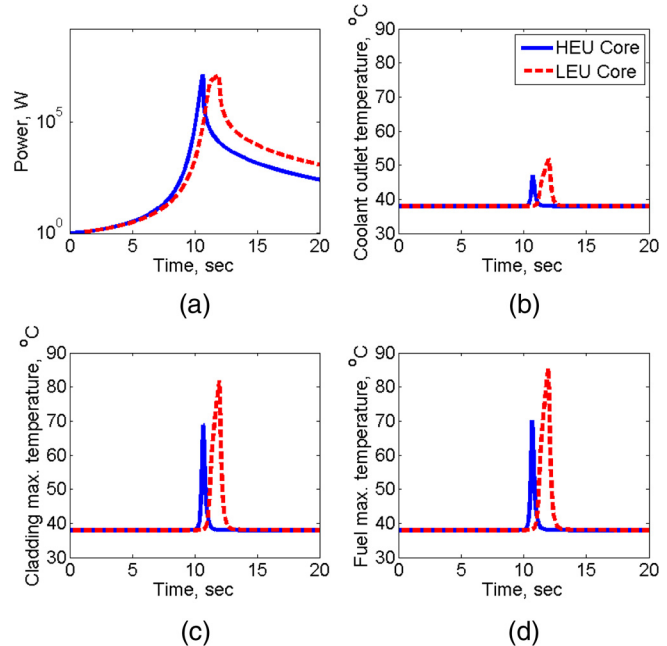


Fig. 13. Transient responses of HEU and LEU benchmark cores to reactivity insertion of 0.1 \$ and 0.09 \$ per 1 s: (a) power, (b) coolant outlet temperature, (c) cladding maximum temperature, and (d) fuel maximum temperature.

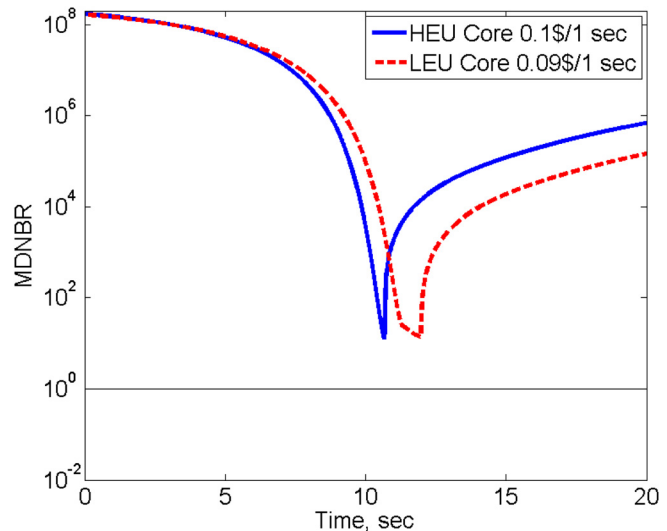


Fig. 14. MCHFR for SRIA transients.

However, THERMO-T uses a power distribution that is obtained by the Serpent full-core three-dimensional neutronic calculation. This power distribution, which is shown in Fig. 15, exhibits lower radial and axial peaking factors, namely, 1.27 and 1.33, respectively, leading to a cooler hot channel and a hotter average channel in the THERMO-T calculations, as compared with the other codes. Nevertheless, the reactivity feedbacks remain practically the same in all codes, as indicated by the

TABLE III
HEU and LEU Cores During FRIA Transients*

Code Institute		THERMO-T BGU	RELAP5 UPISA	PARET ANL	RETRAC LAS	COSTAX JEN	EUREKA JAERI	COBRA Interatom
Trip time (s)	FRIA 1.5 \$/0.5 s for HEU and LEU Cores							
	LEU	0.59	NA	NA	0.57	0.60	0.58	0.57
Power peak (MW)	HEU	0.63	NA	NA	0.61	0.61	0.62	0.61
	LEU	151.3 (0.60)	150.4 (0.61)	148.3 (0.61)	141.1 (0.61)	116.1 (0.64)	143.8 (0.62)	143.9 (0.61)
Clad surface	HEU	128.1 (0.65)	131.2 (0.66)	129.0 (0.66)	128.4 (0.66)	132.7 (0.66)	114.8 (0.66)	135.1 (0.65)
	Temperature Peaks (°C)							
Coolant outlet	LEU	149.5 (0.62)	166.5 (0.63)	155.8 (0.63)	155.9 (0.63)	156.6 (0.63)	149.2 (0.63)	168.2 (0.63)
	HEU	148.92 (0.67)	163.41 (0.67)	155.25 (0.67)	162.04 (0.67)	162.30 (0.68)	147.30 (0.68)	160.00 (0.66)
Clad surface	LEU	78.4 (0.68)	78.0 (0.73)	82.0 (0.71)	79.4 (0.71)	80.4 (0.71)	62.7 (0.76)	63.20 (0.74)
	HEU	79.6 (0.73)	78.9 (0.77)	84.3 (0.76)	83.0 (0.75)	108.7 (0.77)	62.3 (0.82)	70.7 (0.78)
Trip time (s)	FRIA 1.35 \$/0.5 s for LEU Core							
	LEU	0.67	NA	NA	0.66	0.69	0.66	0.65
Power peak (MW)	LEU	64.1 (0.68)	64.4 (0.69)	62.4 (0.69)	63.2 (0.69)	51.8 (0.73)	61.5 (0.70)	62.9 (0.69)
	Temperature Peaks (°C)							
Clad surface	LEU	98.8 (0.72)	113.2 (0.72)	108.01 (0.72)	108.0 (0.72)	102.1 (0.76)	107.2 (0.72)	105.1 (0.71)
	LEU	54.8 (0.78)	56.2 (0.83)	56.9 (0.80)	58.2 (0.83)	54.9 (0.84)	55.20 (0.83)	52.00 (0.84)

*The number in parentheses is the time after transient initiation at which the value occurred.

good agreement in the power level evolution between THERMO-T and the other codes. On the other hand, in the SRIA cases, the differences in cladding temperatures are much smaller, possibly due to lower power levels during these transients, which result from a slower power rise.

IV.B. LOFA Results

The LOFA is initiated at a core power level of 12 MW, which allows including a 20% overpower in the transient scenario. The flow decays exponentially according to

$$Q = Q_0 e^{(-t/\tau)}, \quad (33)$$

where the scram is initiated at 85% of the initial flow. However, the insertion occurs only 0.2 s after the 85% set point is reached. The flow then continues to decay until it reaches 15% of the nominal flow, where it remains until the end of the transient. The decay of the coolant flow is followed by an increase in temperature of the fuel, cladding, and coolant. Two types of LOFA transients are examined, as specified in Table II: a FLOFA, in which the flow decays with a period of 1 s, and a SLOFA, in which the flow decays with a period of 25 s. The results of the FLOFA and SLOFA are shown in Figs. 16 and 17, respectively. The results for all the transient cases are summarized and compared to other codes in Table V.

TABLE IV
HEU and LEU Cores During SRIA Transients*

Code Institute	THERMO-T BGU	RELAP5 UPISA	PARET ANL	RETRAC LAS	COSTAX JEN	EUREKA JAERI	COBRA Interatom
SRIA 0.1 \$/1 s for HEU Core							
Trip time (s)	10.66	NA	NA	10.62	10.61	10.64	10.57
Power peak (MW)	13.2 (10.66)	13.7 (10.65)	14.2 (10.62)	14.1 (10.64)	14.9 (10.64)	13.75 (10.67)	14.4 (10.59)
Temperature Peaks (°C)							
Clad surface	68.9 (10.68)	71.7 (10.66)	69.7 (10.64)	69.0 (10.66)	69.5 (10.66)	69.2 (10.69)	69.2 (10.62)
Coolant outlet	47.0 (10.73)	48.0 (10.74)	47.8 (10.71)	48.1 (10.74)	47.5 (10.73)	47.7 (10.77)	45.2 (10.70)
After 20 s							
Power (MW)	0.0058	0.0078	0.0053	0.0054	0.007	0.006	NA
Temperatures (°C)							
Clad surface	38.0	38.0	38.0	38.0	38.0	38.0	38.0
Coolant outlet	38.0	38.0	38.0	38.0	38.0	38.0	38.0
SRIA 0.09 \$/1 s for LEU Core							
Trip time (s)	10.66	NA	NA	11.87	11.68	11.90	12.028
Power peak (MW)	12.2 (12.26)	12.3 (11.94)	12.2 (11.80)	12.4 (11.89)	13.0 (11.71)	12.4 (11.92)	12.2 (12.053)
Temperature Peaks (°C)							
Clad surface	81.7 (12.27)	81.1 (11.95)	77.9 (11.81)	77.7 (11.90)	71.9 (11.90)	78.5 (11.93)	78.1 (12.06)
Coolant outlet	51.8 (12.30)	53.6 (11.99)	53.0 (11.86)	53.9 (11.93)	48.8 (11.78)	52.8 (11.98)	51.1 (12.10)
After 20 s							
Power (MW)	0.0156	0.0220	0.0121	0.0146	0.0092	0.0150	NA
Temperatures (°C)							
Clad surface	38.0	38.0	38.0	38.0	38.0	38.0	38.0
Coolant outlet	38.0	38.0	38.0	38.0	38.0	38.0	38.0

*The number in parentheses is the time after transient initiation at which the value occurred.

As shown in Fig. 16, the power begins to drop immediately with the reduction in flow rate due to the negative reactivity feedback resulting from a fuel and coolant temperature increase. The scram is initiated when the coolant flow reaches 85% of the initial flow and results in a sharp decrease in core power. A second peak in fuel, cladding, and coolant temperatures is reached a few seconds later as a result of the combined effect of a relatively constant decay heat level

and a continuous reduction in the core coolant flow. The same phenomenon is exhibited in the SLOFA transient, as can be seen in Fig. 17, but on a much slower timescale.

Finally, as can be seen in Table V, the results obtained from the THERMO-T calculations are in good agreement with the results obtained from the other codes provided in the benchmark problem, both for the FLOFA and for the SLOFA. The calculation showed that no boiling occurred

water	graphite	graphite	graphite	graphite	water		
water	4.21±0.015	3.89±0.011	3.88±0.012	4.22±0.014	water	LEU BOL LEU EOL HEU BOL HEU EOL	
	4.27±0.014	3.90±0.012	3.90±0.012	4.26±0.020			
	4.19±0.006	3.91±0.011	3.91±0.011	4.19±0.018			
	4.25±0.014	3.92±0.012	3.92±0.012	4.26±0.013			
4.04±0.011	3.29±0.013	4.52±0.012	4.52±0.012	3.31±0.012	4.06±0.011		
4.10±0.014	3.31±0.014	4.45±0.014	4.44±0.011	3.31±0.013	4.09±0.014		
3.99±0.012	3.69±0.012	4.37±0.003	4.37±0.003	3.69±0.012	3.99±0.012		
4.05±0.014	3.67±0.019	4.30±0.013	4.30±0.015	3.67±0.013	4.04±0.014		
3.46±0.020	3.75±0.015	2.81±0.014	water	2.81±0.015	3.76±0.010		3.47±0.013
3.47±0.010	3.70±0.016	2.76±0.013		2.76±0.013	3.72±0.012		3.47±0.010
3.34±0.012	3.71±0.012	2.63±0.010		2.63±0.010	3.70±0.012	3.32±0.012	
3.45±0.010	3.64±0.014	2.57±0.013		2.56±0.018	3.63±0.012	3.45±0.010	
4.05±0.014	3.30±0.017	4.51±0.014	4.52±0.012	3.31±0.012	4.06±0.011		
4.09±0.012	3.31±0.013	4.45±0.011	4.46±0.012	3.32±0.013	4.11±0.014		
4.00±0.009	3.69±0.012	4.37±0.003	4.39±0.019	3.70±0.012	4.00±0.009		
4.04±0.014	3.67±0.019	4.29±0.021	4.30±0.015	3.67±0.013	4.04±0.014		
water	4.21±0.015	3.89±0.015	3.90±0.013	4.23±0.011	water		
	4.25±0.014	3.90±0.013	3.91±0.013	4.29±0.013			
	4.19±0.006	3.92±0.004	3.92±0.004	4.19±0.006			
	4.25±0.014	3.91±0.015	3.91±0.012	4.26±0.017			
water	graphite	graphite	graphite	graphite	water		

Fig. 15. Power distribution for HEU and LEU cores calculated by Serpent (Ref. 44).

during the SLOFA and FLOFA transients, as can be seen in Fig. 18.

V. CONCLUSIONS

This paper presents a summary report on the development of a three-dimensional coupled NK and TH system code package, which is based on the Serpent/DYN3D/

THERMO-T codes. The first stage in this work was a comprehensive comparison and verification of the Serpent and DYN3D codes against the static results of the IAEA 10-MW(thermal) MTR benchmark,²⁹ which showed excellent agreement.^{28,35} The second stage was a verification of the current transient model against available transient results.^{8,30}

The neutronic and TH models, implemented in the THERMO-T code, are presented, including the decay heat

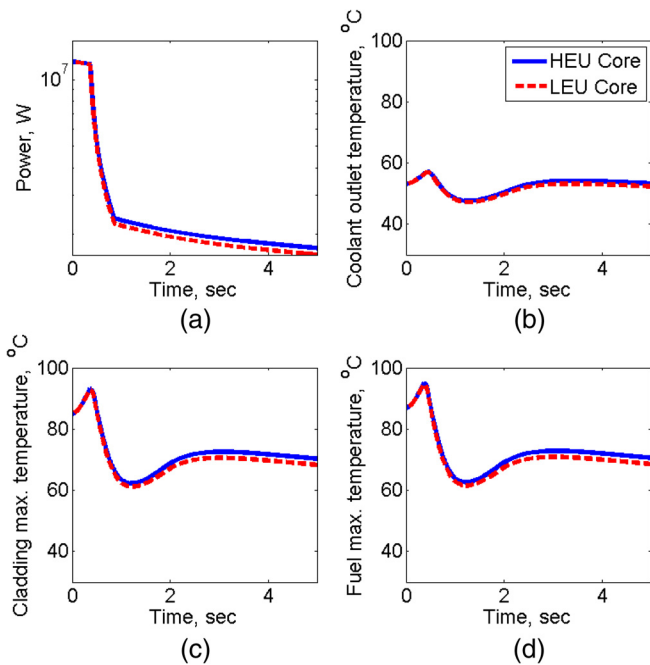


Fig. 16. Transient responses of HEU and LEU benchmark cores to FLOFA: (a) power, (b) coolant outlet temperature, (c) cladding maximum temperature, and (d) fuel maximum temperature.

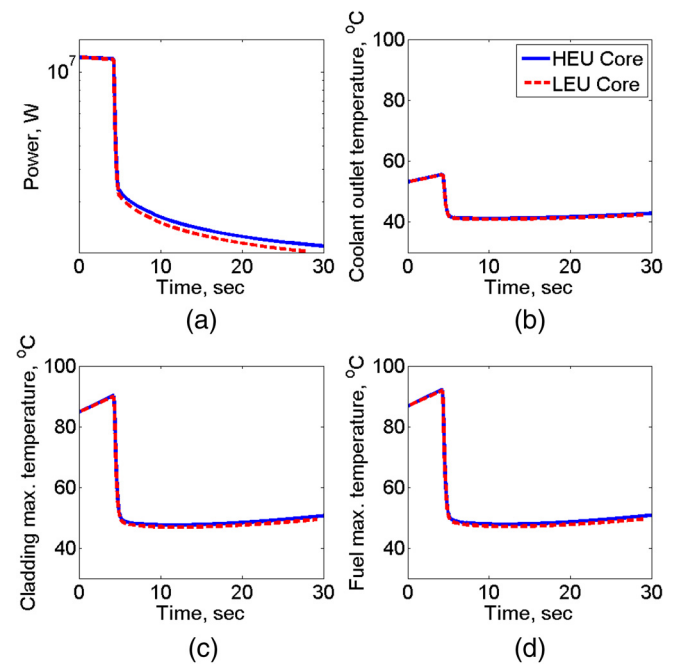


Fig. 17. Transient responses of HEU and LEU benchmark cores to SLOFA: (a) power, (b) coolant outlet temperature, (c) cladding maximum temperature, and (d) fuel maximum temperature.

TABLE V
HEU and LEU Cores in FLOFA and SLOFA Transient Conditions*

Code Institute		THERMO-T BGU	RELAP5 UPISA	PARET ANL	RETRAC LAS	COSTAX JEN	EUREKA JAERI	COBRA Interatom	
Power at trip (MW)	FLOFA for HEU and LEU Cores								
	HEU	11.8	11.9	11.8	NA	11.7	NA	11.5	
	LEU	11.7	11.8	11.7	NA	11.7	NA	11.4	
	Temperature Peaks (°C)								
	Clad surface	HEU	93.4 (0.38)	91.3 (0.41)	88.6 (0.38)	87.5 (0.38)	94.0 (0.37)	98.4 (0.40)	89.5 (0.38)
		LEU	93.0 (0.38)	92.6 (0.4)	88.5 (0.39)	87.5 (0.37)	93.9 (0.37)	97.1 (0.40)	89.3 (0.36)
	Coolant outlet	HEU	57.1 (0.45)	59.5 (0.50)	60.0 (0.47)	60.3 (0.45)	59.4 (0.43)	58.1 (0.48)	56.5 (0.46)
		LEU	56.9 (0.44)	59.5 (0.50)	60.0 (0.48)	60.3 (0.45)	59.3 (0.43)	58.1 (0.48)	56.4 (0.46)
	Temperatures at 15% Flow (°C)								
	Coolant outlet	HEU	49.2	46.8	NA	46.6	NA	NA	NA
LEU		49.2	46.7	NA	46.50	NA	NA	NA	
Power at trip (MW)	SLOFA for HEU and LEU Cores								
	HEU	11.8	11.6	11.6	NA	11.8	NA	11.6	
	LEU	11.7	11.6	11.6	NA	11.7	NA	11.5	
	Temperature Peaks (°C)								
	Clad surface	HEU	90.3 (4.27)	88.7 (4.31)	84.5 (4.30)	83.9 (4.29)	90.7 (4.27)	96.4 (4.20)	85.8 (4.26)
		LEU	89.9 (4.26)	88.4 (4.30)	84.4 (4.07)	83.7 (4.29)	90.3 (4.27)	96.1 (4.30)	85.5 (4.26)
	Coolant outlet	HEU	55.6 (4.29)	58.8 (4.31)	58.7 (4.27)	58.9 (4.29)	58.3 (4.27)	57.7 (4.30)	55.6 (4.26)
		LEU	55.5 (4.28)	58.0 (4.30)	58.7 (4.09)	58.8 (4.29)	58.1 (4.27)	57.5 (4.30)	55.4 (4.26)
	Temperatures at 15% Flow (°C)								
	Coolant outlet	HEU	42.2	43.4	42.2	43.3	NA	NA	NA
LEU		41.8	43.5	NA	43.3	NA	NA	NA	

*The number in parentheses is the time after transient initiation at which the value occurred.

model and the heat transfer model. The models extend lumped-parameter models^{21,43} to nodal solution of two-dimensional (axial coolant flow and radial heat conduction into the fuel) heat transfer equations. Furthermore, to provide a more precise solution, the energy balance equation was coupled with the solution of the mass and momentum conservation equations by utilizing the SIMPLE algorithm.⁴² Several additional features, which

are implemented in the code, are presented, such as the capability to predict the CHF by utilizing the 2006 lookup tables⁴⁹ and solution of the multichannel problem, which includes convergence of the mass flow rate distribution.

The results presented in this paper indicate a fairly good agreement between THERMO-T and the other codes presented in the benchmark.^{8,30} The main difference in the

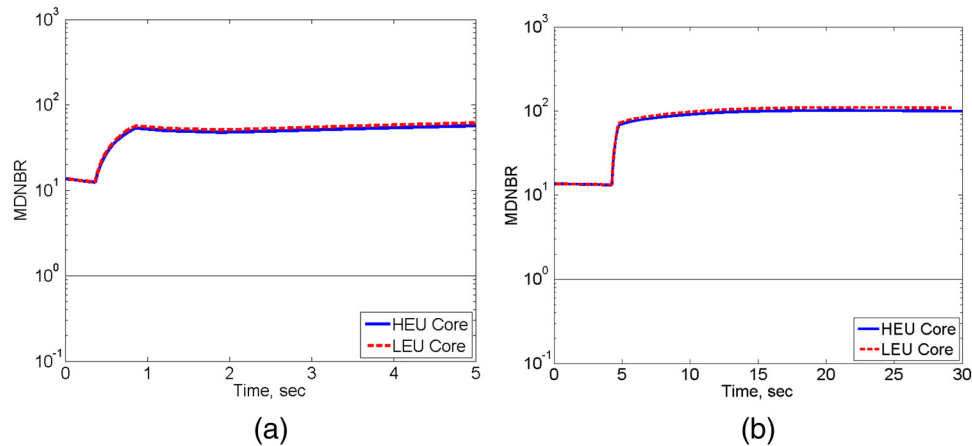


Fig. 18. Minimum DNBR for (a) FLOFA transients and (b) SLOFA transients.

results is observed in the FRIA (see Table III) and is explained by the slightly different peaking factors presented in the benchmark problem and those calculated by Serpent. The differences are dramatically reduced in the slower reactivity insertions due to the slower response of the system, as shown in Table IV for the SRIA. The same behavior is observed in the SLOFA and FLOFA transients, which show good agreement between THERMO-T and the other codes.

Future work should include validation of the THERMO-T code against experimental data. Such a comparison should provide a stronger validity for the utilization of THERMO-T as a modeling tool for transient analysis in the final Serpent/DYN3D/THERMO-T package.

References

1. "IAEA Research Reactor Data Base," International Atomic Energy Agency (2015).
2. F. D'AURIA and A. BOUSBIA-SALAH, "Accident Analysis in Research Reactors," *Proc. 15th Pacific Basin Nuclear Conf.*, Sydney, Australia, October 15–20, 2006, p. 88 (2006).
3. T. HAMIDOUICHE et al., "Overview of Accident Analysis in Nuclear Research Reactors," *Prog. Nucl. Energy*, **50**, 1, 7 (2008); <http://dx.doi.org/10.1016/j.pnucene.2007.11.089>.
4. M. ADORNI et al., "Application of Best Estimate Thermal Hydraulic Codes for the Safety Analysis of Research Reactors," *Proc. Int. Conf. Nuclear Energy for New Europe 2006*, Portoroz, Slovenia, September 18–21, 2006.
5. M. ADORNI et al., "Accident Analysis in Research Reactors," *Proc. Int. Conf. Nuclear Energy for New Europe 2007*, Portoroz, Slovenia, September 10–13, 2007.
6. A. L. COSTA et al., "Safety Studies and General Simulations of Research Reactors Using Nuclear Codes," *Nuclear Power—System Simulations and Operation*, pp. 21–42, P. TSVETKOV, Ed., InTech (2011).
7. "Use and Development of Coupled Computer Codes for the Analysis of Accidents at Nuclear Power Plants," IAEA-TECDOC-1539, International Atomic Energy Agency (2007).
8. T. HAMIDOUICHE et al., "Dynamic Calculations of the IAEA Safety MTR Research Reactor Benchmark Problem Using RELAP5/3.2 Code," *Ann. Nucl. Energy*, **31**, 12, 1385 (2004); <http://dx.doi.org/10.1016/j.anucene.2004.03.008>.
9. A. BOUSBIA-SALAH and F. D'AURIA, "Use of Coupled Code Technique for Best Estimate Safety Analysis of Nuclear Power Plants," *Prog. Nucl. Energy*, **49**, 1, 1 (2007); <http://dx.doi.org/10.1016/j.pnucene.2006.10.002>.
10. W. WOODRUFF et al., "A Comparison of the PARET/ANL and RELAP5/MOD3 Codes for the Analysis of IAEA Benchmark Transients," *Abstracts and Papers of the 1996 Int. RERTR Mtg.*, p. 233, Argonne National Laboratory (Oct. 1996).
11. M. BRETSCHER, N. HANAN, and J. MATOS, "Neutronic Safety Parameters and Transient Analyses for Poland's MARIA Research Reactor," *Abstracts and Papers of the 1999 Int. RERTR Mtg.*, Argonne National Laboratory (Oct. 1999).
12. J. R. DEEN et al., "Neutronic Safety Parameters and Transient Analyses for Potential LEU Conversion of the IR-8 Research Reactor," *Abstracts and Papers of the 1999 Int. RERTR Mtg.*, Argonne National Laboratory (Oct. 1999).
13. M. ADORNI et al., "Analysis of Partial and Total Flow Blockage of a Single Fuel Assembly of an MTR Research Reactor Core," *Ann. Nucl. Energy*, **32**, 15, 1679 (2005); <http://dx.doi.org/10.1016/j.anucene.2005.06.001>.
14. A. HEDAYAT, H. DAVILU, and J. JAFARI, "Loss of Coolant Accident Analyses on Tehran Research Reactor by RELAP5/MOD3.2 Code," *Prog. Nucl. Energy*, **49**, 7, 511 (2007); <http://dx.doi.org/10.1016/j.pnucene.2007.07.009>.

15. Q. LU, S. QIU, and G. SU, "Flow Blockage Analysis of a Channel in a Typical Material Test Reactor Core," *Nucl. Eng. Des.*, **239**, 1, 45 (2009); <http://dx.doi.org/10.1016/j.nucengdes.2008.06.016>.
16. M. AZZOUNE et al., "NUR Research Reactor Safety Analysis Study for Long Time Natural Convection (NC) Operation Mode," *Nucl. Eng. Des.*, **240**, 4, 823 (2010); <http://dx.doi.org/10.1016/j.nucengdes.2009.11.040>.
17. S. CHATZIDAKIS et al., "A Comparative Assessment of Independent Thermal-Hydraulic Models for Research Reactors: The RSG-GAS Case," *Nucl. Eng. Des.*, **268**, 77 (2014); <http://dx.doi.org/10.1016/j.nucengdes.2013.11.076>.
18. S. U.-D. KHAN, S. U.-D. KHAN, and M. PENG, "Flow Blockage Accident or Loss of Flow Accident by Using Comparative Approach of NK/TH Coupling Codes and RELAP5 Code," *Ann. Nucl. Energy*, **64**, 311 (2014); <http://dx.doi.org/10.1016/j.anucene.2013.10.010>.
19. H. V. SOARES et al., "Analysis of Loss of Flow Events on Brazilian Multipurpose Reactor Using the RELAP5 Code," *Int. J. Nucl. Energy*, **2014**, 186189 (2014); <http://dx.doi.org/10.1155/2014/186189>.
20. A. HAINOUN and A. SCHAFFRATH, "Simulation of Subcooled Flow Instability for High Flux Research Reactors Using the Extended Code ATHLET," *Nucl. Eng. Des.*, **207**, 2, 163 (2001); [http://dx.doi.org/10.1016/S0029-5493\(00\)00410-6](http://dx.doi.org/10.1016/S0029-5493(00)00410-6).
21. C. HOUSIADAS, "Simulation of Loss-of-Flow Transients in Research Reactors," *Ann. Nucl. Energy*, **27**, 18, 1683 (2000); [http://dx.doi.org/10.1016/S0306-4549\(00\)00053-0](http://dx.doi.org/10.1016/S0306-4549(00)00053-0).
22. A. BOUSBIA-SALAH and T. HAMIDOUCHE, "Analysis of the IAEA Research Reactor Benchmark Problem by the RETRAC-PC Code," *Nucl. Eng. Des.*, **235**, 6, 661 (2005); <http://dx.doi.org/10.1016/j.nucengdes.2004.10.004>.
23. A. BOUSBIA-SALAH et al., "A Model for the Analysis of Loss of Decay Heat Removal During Loss of Coolant Accident in MTR Pool Type Research Reactors," *Ann. Nucl. Energy*, **33**, 5, 405 (2006); <http://dx.doi.org/10.1016/j.anucene.2005.12.001>.
24. T. HAMIDOUCHE et al., "Application of Coupled Code Technique to a Safety Analysis of a Standard MTR Research Reactor," *Nucl. Eng. Des.*, **239**, 10, 2104 (2009); <http://dx.doi.org/10.1016/j.nucengdes.2009.06.002>.
25. S. S. ARSHI, H. KHALAFI, and S. MIRVAKILI, "Preliminary Thermal-Hydraulic Safety Analysis of Tehran Research Reactor During Fuel Irradiation Experiment," *Prog. Nucl. Energy*, **79**, 32 (2015); <http://dx.doi.org/10.1016/j.pnucene.2014.10.009>.
26. A. BOUSBIA-SALAH et al., "MTR Benchmark Static Calculations with MCNP5 Code," *Ann. Nucl. Energy*, **35**, 5, 845 (2008); <http://dx.doi.org/10.1016/j.anucene.2007.09.016>.
27. K. S. CHAUDRI and S. M. MIRZA, "Burnup Dependent Monte Carlo Neutron Physics Calculations of IAEA MTR Benchmark," *Prog. Nucl. Energy*, **81**, 43 (2015); <http://dx.doi.org/10.1016/j.pnucene.2014.12.018>.
28. M. MARGULIS and E. GILAD, "Monte Carlo and Nodal Neutron Physics Calculations of the IAEA MTR Benchmark Using Serpent/DYN3D Code System," *Prog. Nucl. Energy*, **88**, 118 (2016); <http://dx.doi.org/10.1016/j.pnucene.2015.12.008>.
29. "Research Reactor Core Conversion from the Use of High-Enriched Uranium to the Use of Low Enriched Uranium Fuels Guidebook," IAEA-TECDOC-233, International Atomic Energy Agency (1980).
30. "Research Reactor Core Conversion Guidebook," IAEA-TECDOC-643, International Atomic Energy Agency (1992).
31. P. K. ROMANO and B. FORGET, "The OpenMC Monte Carlo Particle Transport Code," *Ann. Nucl. Energy*, **51**, 274281 (2013); <http://dx.doi.org/10.1016/j.anucene.2012.06.040>.
32. J. LEPPANEN, "Development of a New Monte Carlo Reactor Physics Code," PhD Thesis, Helsinki University of Technology (2007).
33. J. LEPPANEN et al., "The Serpent Monte Carlo Code: Status, Development and Applications in 2013," *Ann. Nucl. Energy*, **82**, 142 (2015); <http://dx.doi.org/10.1016/j.anucene.2014.08.024>.
34. G. MARLEAU, A. HEBERT, and R. ROY, "A User Guide for DRAGON Version DRAGON 0000331 Release 3.04," PhD Thesis, Institute de genie nucleaire, Ecole Polytechnique de Montreal (2000).
35. M. MARGULIS, Y. SHAPOSHNIC, and E. GILAD, "IAEA 10 MW MTR Benchmark: Static Calculation with SERPENT Code," *Proc. 4th Int. SERPENT User Group Mtg.*, Cambridge, United Kingdom, September 17–19, 2014.
36. Y. SHAPOSHNIK, E. SHWAGERAUS, and E. ELIAS, "Thermal-Hydraulic Feedback Module for BGCore System," PhD Thesis, Department of Nuclear Engineering, Ben Gurion University of the Negev (2008).
37. M. MARGULIS and E. SHWAGERAUS, "Extending Two-Phase Capabilities of Thermal-Hydraulic Module in BGCore," *Proc. 27th Conf. Nuclear Societies in Israel*, Dead Sea, Israel, February 11–13, 2014.
38. D. KOTLYAR et al., "Coupled Neutronic Thermo-Hydraulic Analysis of Full PWR Core with Monte-Carlo Based BGCore System," *Nucl. Eng. Des.*, **241**, 9, 37773786 (2011); <http://dx.doi.org/10.1016/j.nucengdes.2011.07.028>.
39. D. KOTLYAR and E. SHWAGERAUS, "Numerically Stable Monte Carlo-Burnup-Thermal Hydraulic Coupling Schemes," *Ann. Nucl. Energy*, **63**, 371381 (2014); <http://dx.doi.org/10.1016/j.anucene.2013.08.016>.
40. Y. BILODID et al., "Spectral History Model in DYN3D: Verification Against Coupled Monte-Carlo Thermal-Hydraulic Code BGCore," *Ann. Nucl. Energy*, **81**, 3440 (2015); <http://dx.doi.org/10.1016/j.anucene.2015.03.030>.

41. D. KOTLYAR, E. FRIDMAN, and E. SHWAGERAUS, "Coupled Neutronic Thermo-Hydraulic Analysis of Full PWR Core with BGCORE System," *Proc. Annual Mtg. Nuclear Technology*, Dresden, Germany, May 12–14, 2009.
42. H. K. VERTSTEEG and W. MALALASEKERA, *An Introduction to Computational Fluid Dynamics: The Finite Volume Method*, Longman Scientific and Technical (1995).
43. M. A. GAHEEN et al., "Simulation and Analysis of IAEA Benchmark Transients," *Prog. Nucl. Energy*, **49**, 3, 217 (2007); <http://dx.doi.org/10.1016/j.pnucene.2006.12.003>.
44. M. MARGULIS and E. GILAD, "Analysis of Protected RIA and LOFA in Plate Type Research Reactor Using Coupled Neutronics Thermal-Hydraulics System Code," *Proc. 16th Int. Topl. Mtg. Nuclear Reactor Thermal Hydraulics (NURETH-16)*, Chicago, Illinois, August 30–September 4, 2015, American Nuclear Society (2015).
45. U. GRUNDMANN, U. ROHDE, and S. MITTAG, "DYN3D—Three-Dimensional Core Model for Steady State and Transient Analysis of Thermal Reactors," *Proc. PHYSOR 2000—Advances in Reactor Physics and Mathematics and Computation into the Next Millennium*, Pittsburgh, Pennsylvania, May 7–11, 2000, American Nuclear Society (2000).
46. U. GRUNDMANN, U. ROHDE, and S. MITTAG, "DYN3D Version 3.2 Code for Calculation of Transients in Light Water Reactors (LWR) with Hexagonal or Quadratic Fuel Elements Description of Models and Methods," FZR-434, Helmholtz-Zentrum Dresden-Rossendorf (2005).
47. G. R. KEEPIN, *Physics of Nuclear Kinetics*, Addison-Wesley (1965).
48. M. J. McGUIRE, "An Analysis of the Proposed MITR-III Core to Establish Thermal-Hydraulic Limits at 10 MW," PhD Thesis, Massachusetts Institute of Technology (1995).
49. D. GROENEVELD et al., "The 2006 CHF Look-Up Table," *Nucl. Eng. Des.*, **237**, 1909 (2007); <http://dx.doi.org/10.1016/j.nucengdes.2007.02.014>.
50. N. KOLEV, "Check of the 2005-Look Up Tables for Prediction of CHF in Bundles," *Nucl. Eng. Des.*, **237**, 9, 978 (2007); <http://dx.doi.org/10.1016/j.nucengdes.2006.10.021>.
51. M. E. NAKLA et al., "Application of the Critical Heat Flux Look-Up Table to Large Diameter Tubes," *Sci. Technol. Nucl. Install.*, **2013**, 868163 (2013); <http://dx.doi.org/10.1155/2013/868163>.
52. N. TODREAS and M. KAZIMI, *Nuclear Systems I: Thermal Hydraulic Fundamentals*, Taylor & Francis (1990).
53. M. HOLMGREN, "X Steam: Thermodynamic Properties of Water and Steam" (2006); <http://www.mathworks.com/matlabcentral/fileexchange/9817-x-steam-thermodynamic-properties-of-water-and-steam> (current as of Aug. 24, 2016).
54. "IAPWS Industrial Formulation 1997 for the Thermodynamic Properties of Water and Steam," IAPWS-IF97, International Association for the Properties of Water and Steam.